Preparation and Electrocatalytic Study of Myoglobin Biosensor Based on Platinum-Gold-Three Dimensional Graphene Modified Electrode

Bo Shao, Wei Chen, Lijun Yan, Yuhao Huang, Bei Wang, Qingwu Zou, Yongkang Xuan, Wei Sun[*], Yanyan Niu[*]

Key Laboratory of Laser Technology and Optoelectronic Functional Materials of Hainan Province, Key Laboratory of Functional Materials and Photoelectrochemistry of Haikou, College of Chemistry and Chemical Engineering, Hainan Normal University, Haikou 571158, China
[*]E-mail: sunwei@hainnu.edu.cn, niuyanyan171006@hainnu.edu.cn

An electrochemical biosensor was prepared by using platinum-gold-three dimensional graphene (Pt-Au-3DGR) and myoglobin (Mb) with ionic liquid N-hexylpyridinium hexafluorophosphate modified carbon paste electrode (CILE) as the base electrode. The mixed materials of Pt-Au-3DGR and Mb were modified on the electrode to obtain the electrochemical biosensor (Nafion/Mb/Pt-Au-3DGR/CILE). The synthesized Pt-Au-3DGR was characterized by scanning electron microscopy and transmission electron microscopy, which showed a three-dimensional cobweb structure of GR with Pt-Au bimetal successfully loaded on its structure. The biostructure of Mb was analyzed by UV-Vis spectroscopy and infrared spectroscopy. Direct electrochemistry and electrocatalytic behaviors of this biosensor were tested by cyclic voltammetry and electrochemical impedance spectroscopy, which were further compared with the control group. The results prove that Nafion/Mb/Pt-Au-3DGR/CILE has obvious electrocatalytic functions to trichloroacetic acid (TCA) and sodium nitrite (NaNO$_2$). The linear ranges for TCA and NaNO$_2$ are 1.0-30.0 mmol L^{-1} and 0.05-0.55 mmol L^{-1} with the detection limits as 0.33 mmol L^{-1} and 0.01 mmol L^{-1}, respectively.

1. INTRODUCTION

Myoglobin (Mb) is a kind of heme monomer protein, which mainly exists in the heart and striated muscle of vertebrates [1]. In organisms Mb can store oxygen [2], promote oxygen transport in cells [3], catalyze nitrite to produce nitric oxide for heart balance, and protect the heart from damage [4, 5]. Due to the presence of iron porphyrin as electroactive center of Mb, it can be used to prepare third generation biosensor. However, Mb has a large and complex multipolar polypeptide chain

structure, which deeply encloses the redox center, inhibiting the interaction between the electroactive center and electrode seriously [6]. Accordingly, different materials have been used to form thin films for loading protein, which can not only provide a favorable microenvironment for protein immobilization, but also enhance the direct electron transfer between protein and electrode [7]. Niu et al. synthesized TiO_2-doped carbon nanofiber composite to study hemoglobin electrocatalysis [8]. Luo et al. investigated the detection of trichloroacetic acid (TCA) with Nafion/Mb/AuNPs/Mg-MOF-74/CILE [9].

Nanomaterials have been widely applied to photocatalysis and electrocatalysis due to their unique physical and chemical properties [10]. The excellent conductivity and catalytic activity of gold and platinum make them more attractive for sensor applications [11, 12]. Multicomponent nanocomposites have different or complementary physical and chemical properties under certain conditions, which can interact synergistically and improve the response performance of devices [13]. Anyar et al. used platinum-silver-graphene (GR) composite modified electrode to realize the detection of dopamine at low concentration [14].

As a two-dimensional material, GR has shown excellent advantages in the field of sensors with large specific surface area and unique electrochemical properties [15]. However, the intense π-π stacking between graphite layers leads to irreversible agglomeration in actual use, which leads to a sharp decrease in specific surface area and conductivity [16, 17]. In order to solve this problem, researchers used electrochemical method [18], hydrothermal method [19], vapor deposition [20] and other methods to assemble two-dimensional GR sheets into three-dimensional porous structures. The obtained three-dimensional GR (3DGR) not only keeps the excellent physical and chemical properties of 2DGR, but also prevents the stacking to a great extent due to the formation of three-dimensional network structure. In general 3DGR has larger specific surface area, more excellent conductivity and mass transfer ability [21]. Also 3D-turned GR is easier to combine with other nanomaterials and exhibits broader application prospects in catalysis, energy storage, sensors etc., due to the synergistic effects [22].
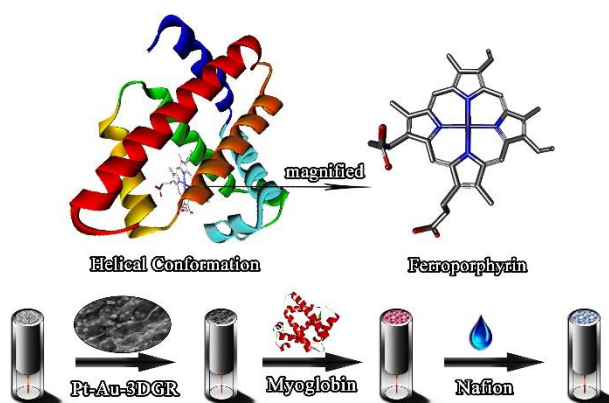
Scheme 1. Helical conformation of Mb and ferroporphyrin, and flowchart of detailed fabrication of Nafion/Mb/Pt-Au-3DGR/CILE.

In this study, we constructed an enzyme electrode based on platinum-gold-3DGR composite, which was synthesized by hydrothermal method. The three-dimensional composite was used to fix Mb and prepared an enzyme electrode with a carbon ionic liquid electrode (CILE) as the base electrode. The flowchart diagram of Mb molecule and the fabrication process of this biosensor are shown in Scheme 1.

2. EXPERIMENTAL

2.1 Apparatus

CHI 604E electrochemical workstation (Shanghai CH Instrument, China) was equipped with a standard three electrode system, including homemade CILE ($\Phi = 4.0$ mm) as the working electrode, platinum electrode as the auxiliary electrode and saturated calomel electrode (SCE) as the reference electrode. Scanning electron microscopy (SEM) images were performed by a JSM-7100F (JEOL, Japan) microscope and transmission electron microscopy (TEM) were recorded with a JEM-2010F (JEOL, Japan) microscope operated at 200 kV. FT-IR was obtained on a Nicolet 6700 FT-IR spectrophotometer (Thermo Fisher Scientific Inc, USA) with UV-vis spectroscopy on a TU-1901 dual-beam ultraviolet-visible spectrophotometer (Beijing Purkay General Co. Ltd., China).

2.2 Reagents

N-Hexylpyridinium hexafluorophosphate (HPPF$_6$, Lanzhou Yulu Fine Chemical Co. Ltd., China), GO solution (8.0 mg mL^{-1}, Shanxi Institute of Coal Chemistry, Chinese Academy of Sciences), HAuCl$_4$ and H$_2$PtCl$_6$ (Tianjin Kaima Biochem. Co. Ltd., China), graphite powder (average particle size ≤ 30 μm, Shanghai Colloidal Chemical Factory, China), Mb (MW:17800, Sinopharm Chemical Reagent Co., Ltd., China), Nafion (5.0 % ethanol solution, Sigma), TCA (Tianjin Kemiou Chem. Co., Ltd., China), NaNO$_2$ (Shanghai Chemical Reagent Factory, China) were used as received and double-distilled water was used as the experimental water. The supporting electrolyte solution was deoxygenated with purified N$_2$ for 45 min to remove O$_2$ before each experiment.

2.3 Fabrication of Nafion/Mb/Pt-Au-3DGR/CILE

CILE was prepared according to the literature [23], specifically as follows: the mixture of graphite powder and HPPF$_6$ with a mass ratio of 2:1 was ground, and then filled into a glass tube tightly (inner $\Phi = 4$ mm). The electrode interface was polished smoothly on polishing paper before decoration.

Pt-Au-3DGR was prepared by a one-step hydrothermal synthesis. In general, 0.25 mL of HAuCl$_4$ (243.3 mmol L^{-1}) and 0.25 mL of H$_2$PtCl$_6$ (243.3 mmol L^{-1}) were mixed with 19.5 mL of 2.0 mg mL^{-1} GO solution and shaked homogeneously. Then 1.0 mL triethylenetetramine was added dropwise under stirring. After that the mixture was put into 50 mL stainless steel reactor, heated at

180 °C for 12 hours, and cooled naturally to obtain the cylindrical gel with the unreacted substances removed by soaking in water. After 12 hours of freeze-drying at -87 °C, the cylindrical Pt-Au-3DGR was obtained.

The modification on CILE was carried out by direct dropping method. 8.0 μL of 0.6 mg·mL^{-1} Pt-Au-3DGR dispersion was dropped on CILE and dried at room temperature. Then 8.0 μL 15.0 mg·mL^{-1} Mb was dropped and dried at room temperature again. Finally, 6.0 μL 0.5 % Nafion ethanol solution was spread on it to obtain Nafion/Mb/Pt-Au-3DGR/CILE. Other electrodes including Nafion/CILE, Nafion/Mb/CILE and Nafion/Pt-Au-3DGR/CILE were fabricated with similar procedure.

3. RESULTS AND DISCUSSION

3.1 Characterization of Pt-Au-3DGR

SEM images of Pt-Au-3DGR are shown in Fig. 1A and 1B with clear cobweb cavity structure. The wrinkled GR is loaded with Pt-Au particles of uniform size inside and on the surface, which resembled as an unopened flower bud at enlarged image (Fig. 1B). TEM of Pt-Au-3DGR is shown in Fig. 1C, which indicated that Pt-Au bimetal were uniformly dispersed inside and outside of 3DGR. The lattices are obvious and easy to be observed in high resolution TEM (Fig. 1D), indicating that Pt-Au bimetal nanomaterial was successfully loaded within the macrostructure of 3DGR.
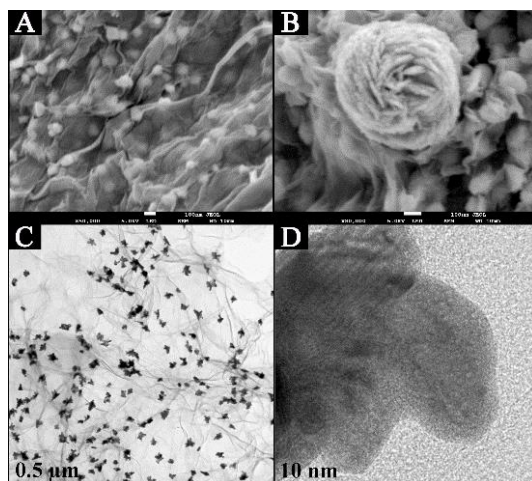

Figure 1. (A, B) SEM images of Pt-Au-3DGR under different magnifications; TEM (C) and HR-TEM (D) images of Pt-Au-3DGR.

3.2 Spectral characterization

The change of Soret band in UV-Vis absorption spectrum can be used to judge whether the molecular structure of biological protein is destroyed [24]. As shown in Fig. 2A, UV-Vis spectra of Mb solution (curve a) and Mb-Pt-Au-3DGR mixed solution (curve b) at pH 3.0 were present with the Soret

band both at 408.00 nm, indicating undamaged biological structure of Mb after mixing with Pt-Au-3DGR. FT-IR spectrum is further used to determine whether the biological protein molecules are denatured or not [25], in which the peak at 1700-1600 cm^{-1} is the C=O stretching vibration peak, and 1600-1500 cm^{-1} is the N-H and C-N bending vibration peak. The amide I and II bands of Mb solution were located at 1650 cm^{-1} and 1540 cm^{-1} (Fig. 2B-b), and the characteristic peaks of Mb-Pt-Au-3DGR appeared at 1650 cm^{-1} and 1530 cm^{-1} (Fig. 2B-a), demonstrating that Mb was not denatured in the presence of Pt-Au-3DGR.
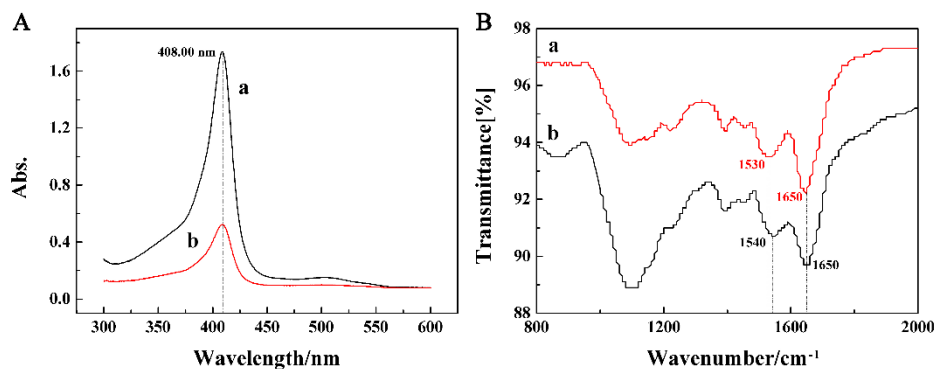
Figure 2. (A) UV-Vis absorption spectra of Mb (curve a) and Mb-Pt-Au-3DGR mixture (curve b) in pH 3.0 buffer; (B) FT-IR spectra of Mb-Pt-Au-3DGR composite film (a) and Mb (b).

3.3 Direct electrochemistry of Mb

Cyclic voltammetric (CV) curves of different modified electrodes in PBS at pH 3.0 are shown in Fig. 3. There are no redox peaks on Nafion/CILE (curve d) and Nafion/Pt-Au-3DGR/CILE (curve c), which proves no electrochemical active substances on the electrode surfaces. With the presence of Pt-Au-3DG on the electrode larger background current appears. Meanwhile, a pair of redox peaks appeared on Nafion/Mb/CILE (curve b) and Nafion/Mb/Pt-Au-3DGR/CILE (curve a), which indicated the success realization of electron exchange between iron porphyrin in Mb and CILE surface. Also, the largest responses of Mb appeared on curve a, indicating the modification of Pt-Au-3DGR on CILE made the redox reaction of Mb more easily, which was due to the improved loading capacity of cobweb-like Pt-Au-3DGR porous structure for Mb. Moreover, Pt-Au-3DGR has high conductivity, large specific surface area and excellent biocompatibility, which accelerates the electron exchange of active center of Mb to electrode. On Nafion/Mb/Pt-Au-3DGR/CILE, E_{pc} and E_{pa} are located at -0.275 V and -0.153 V (*vs.* SCE) with $\triangle E_p$ as 0.124 V, $E^{0'}$ as -0.214 V (*vs.* SCE), and the ratio of redox peak current is 1, which are the characteristic electrochemical behavior of Fe(III)/Fe(II) electric pair of Mb.
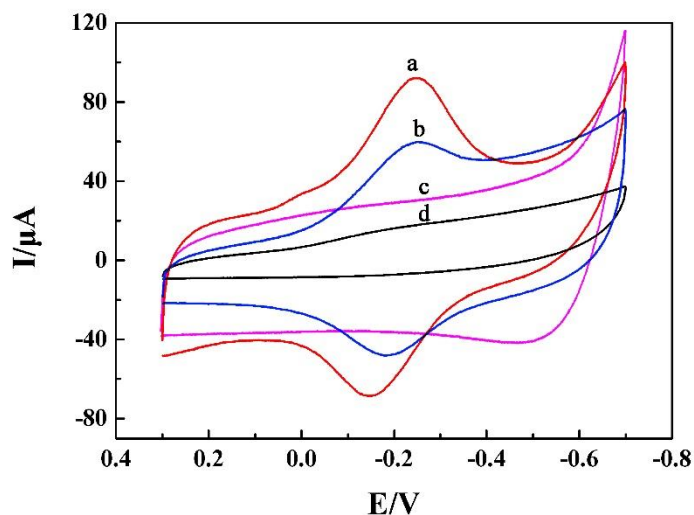
Figure 3. CVs of (a) Nafion/Mb/Pt-Au-3DGR/CILE, (b) Nafion/Mb/CILE, (c) Nafion/Pt-Au-3DGR/CILE, (d) Nafion/CILE in pH 3.0 buffer with scan rate of 0.1 V·s^{-1}.

3.4 EIS results

EIS can effectively reflect the impedance information of electrode interface, and electron transfer resistance (Ret) can be obtained by measuring the diameter corresponding to the half-arc length in high frequency region. Using $[Fe(CN)_6]^{3-/4-}$ as redox probe, EIS of different modified electrodes were investigated with the experimental data fitted by Randles equivalent circuit. As shown in Fig. 4, the Ret values of each electrodes were got as 0 Ω (Nafion/Pt-Au-3DGR/CILE, curve a), 39.01 Ω (Nafion/Mb/Pt-Au-3DGR/CILE, curve b), 55.22 Ω (Nafion/CILE, curve c) and 78.10 Ω (Nafion/Mb/CILE, curve d), respectively. Because Mb is a macromolecule containing polypeptide chain that can increase the interfacial resistance. However, the high conductive Pt-Au-3DGR is benefit for the decrease of the interfical resistance.
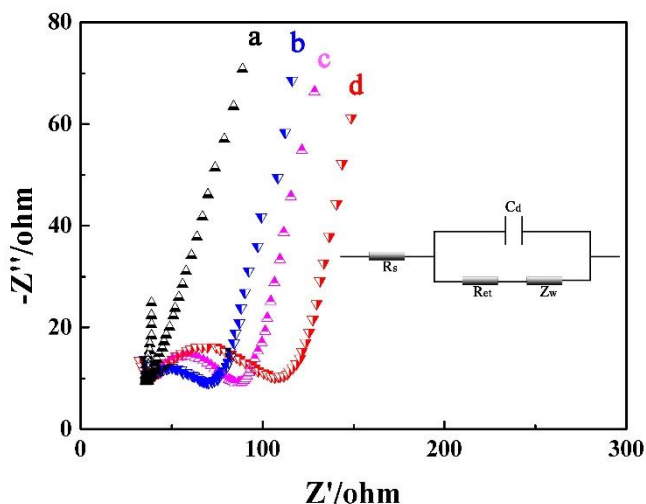
Figure 4. EIS pattern: (a) Nafion/Pt-Au-3DGR/CILE (b) Nafion/Mb/Pt-Au-3DGR/CILE, (c) Nafion/CILE, (d) Nafion/Mb/CILE in a 10.0 mmol·L^{-1} $[Fe(CN)_6]^{3-/4-}$ and 0.1 mol·L^{-1} KCl solution with frequency from 10^4 to 0.1 Hz (Inset is the Randles circuit model in the cell).

3.5 Effect of buffer pH

The effect of pH (3.0-8.0) of PBS on the electrochemical behavior of Nafion/Mb/Pt-Au-3DGR/CILE was further checked with cyclic voltammograms shown in Fig. 5A. The formal potential ($E^{0'}$) gradually shifts to the negative potential with the increase of pH. The linear regression equation of $E^{0'}$ and pH is obtained as $E^{0'}$ (V) = -0.0509 pH +0.033 (n = 6, γ = 0.994) with a slope of -50.9 mV pH^{-1}, slightly smaller than -57.6 mV pH^{-1} of reversible reaction at 291K (theoretical value). It shows that Mb undergoes single electron and single proton transfer on the electrode during electrochemical reaction. According to the reference [26], the equation is expressed as: Mb Fe(III) + H^+ + e $\rightleftharpoons$ Mb Fe(II)。
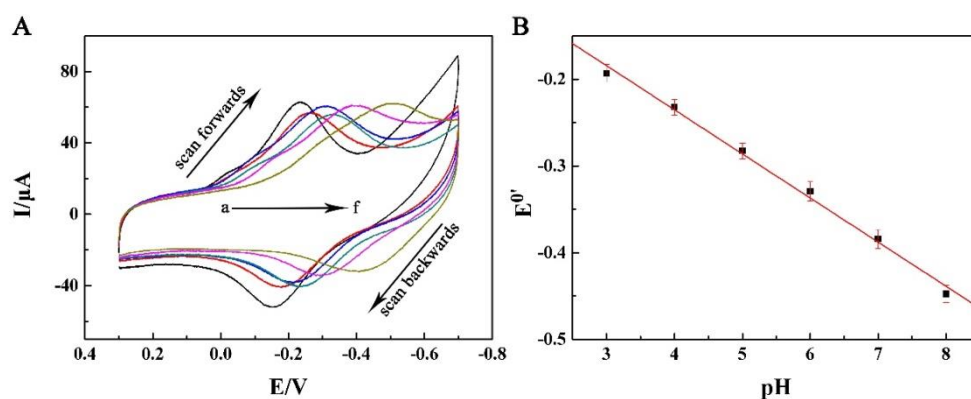


Figure 5. (A) Influence of buffer pH on Nafion/Mb/Pt-Au-3DGR/CILE at scan rate of 0.1 $V·s^{-1}$ (from a to f as 3.0, 4.0, 5.0, 6.0, 7.0, 8.0); (B) Linear relationship of $E^{0'}$ versus pH.

3.6 Electrocatalytic behavior of Nafion/Mb/Pt-Au-3DGR/CILE

CV was used to investigate the catalytic performance for TCA at different concentrations in pH 3.0 PBS. As shown in Fig. 6A, the reduction peak current at -0.286 V increases and a new reduction peak appears at -0.518 V with the increase of TCA concentration, meanwhile the oxidation peak current decreases and finally disappears, indicating that electrocatalytic reaction occurs. A good linear relationship between reduction peak current and TCA concentration was got in the range of 1.0~30.0 $mmol·L^{-1}$ with the linear regression equation as I (μA) = 4.426 C ($mmol·L^{-1}$) + 21.57 (n = 9, γ= 0.996) and the detection limit as 0.33 $mmol·L^{-1}$ (3σ). When the concentration of TCA is more than 30.0 $mmol·L^{-1}$, the reduction current peak tends to be stable, which indicates that the reaction process is in accordance with Michaelis-Menten kinetic equation. The apparent Michaelis constant (K_M^{app}) is used to understand the catalytic effect of Mb on the modified electrode. Based on the electrochemical form of Lineweaver-Burk equation [27], the K_M^{app} was calculated as 15.97 $mmol·L^{-1}$.

Meanwhile, electrocatalysis to $NaNO_2$ was studied by cyclic voltammetry with the results shown in Fig. 6B. The reduction peak current increases with the increase of $NaNO_2$ concentration and further a new reduction peak appears near to -0.665 V. The linear regression equation is obtained as I(μA) = 115.56 C ($mmol·L^{-1}$) +1.03 (n = 12, γ = 0.996) in the concentration range of 0.05~0.55

mmol·L^{-1} with the detection limit as 0.01 mmol·L^{-1} (3σ) and K_M^{app} as 9.51 mmol·L^{-1}. Therefore Nafion/Mb/Pt-Au-3DGR/CILE also has good electrochemical response to NaNO$_2$.
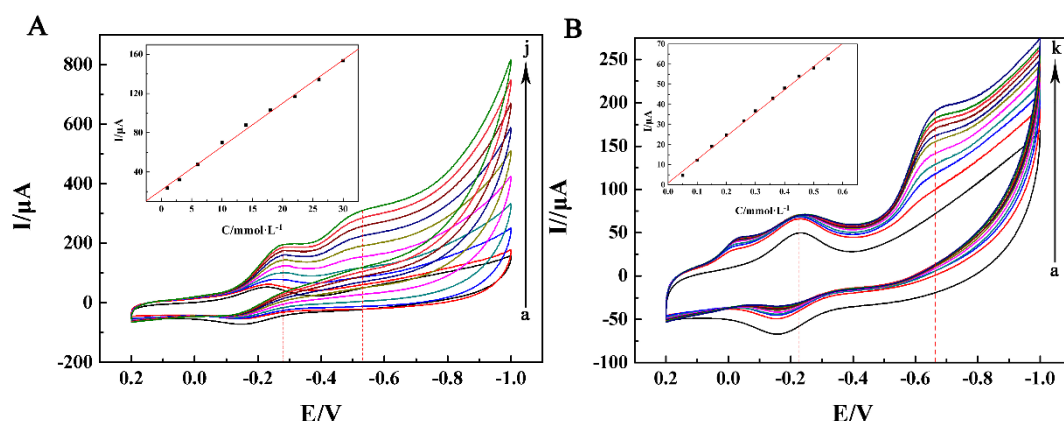
Figure 6. (A) CVs of Nafion/Mb/Pt-Au-3DGR/CILE with different C$_{TCA}$ (from a to j as 0.0, 1.0, 3.0, 6.0, 10.0, 14.0, 18.0, 22.0, 26.0, 30.0 mmol·L^{-1}; inset is the linear relationship of Ipc versus TCA concentration); (B) CVs of Nafion/Mb/Pt-Au-3DGR/CILE with different C$_{NaNO_2}$ (from a to k as 0.05, 0.10, 0.15, 0.20, 0.26, 0.30, 0.36, 0.40, 0.45, 0.50, 0.55 mmol·L^{-1}; inset is the linear relationship of Ipc versus NaNO$_2$ concentration).

Table 1. Comparison of electrocatalytic detection of TCA and NaNO$_2$ on different modified electrodes

Electrodes	Analytes	Linear range (mmol·L^{-1})	Detection limit (mmol·L^{-1})	K_M^{app} (mmol·L^{-1})	Ref.
Nafion/Mb/BN/CILE	TCA	0.2 - 30.0	0.05	/	26
Mb-SGO-Nafion/GCE	NaNO$_2$	2.0 - 24.5	1.5	/	28
Nafion/Mb/GT/CILE	TCA	3.0 - 180.0	1.0	4.88	29
	NaNO$_2$	0.4 - 4.2	0.133	1.358	
Nafion/Mb-SA-TiO$_2$/CILE	TCA	5.3 - 114.2	0.152	32.3	30
Nafion/Mb/ZnO@3DGR/CILE	TCA	0.5 - 30.0	0.167	1.78	31
Nafion/Mb/C$_3$N$_4$/CILE	TCA	4.0 - 64.0	1.33	7.83	32
Nafion/Mb-HAp@CNF/CILE	TCA	6.0 - 180.0	2.0	0.224	33
	NaNO$_2$	0.3 - 10.0	0.23	1.13	
Nafion/Mb/Au-BC/CILE	TCA	4.0 - 240.0	1.33	78.5	34
	NaNO$_2$	1.0 - 30.0	0.33	7.14	
Nafion/Hb/Co$_3$O$_4$-CNF/CILE	NaNO$_2$	1.0 - 12.0	0.33	-	35
Nafion/Mb/Pt-Au-3DGR/CILE	TCA	1.0 - 30.0	0.33	15.97	This work
	NaNO$_2$	0.05 - 0.55	0.01	9.51	

BN: boron nitride; SGO: sulfonated graphene oxide; GT: graphene tube; SA: sodium alginate; HAp@CNF: hydroxyapatite doped carbon nanofiber; BC: biomass carbon; CNF: carbon nanofiber.

A systematic comparison of this electrochemical Mb sensor with other protein modified electrodes for TCA and/or NaNO$_2$ detection was summarized in table 1, which indicated that

Nafion/Mb/Pt-Au-3DGR/CILE was suitable for low concentration quantitative analysis with lower detection limit.

4. CONCLUSION

   In this paper, an electrochemical Mb biosensor (Nafion/Mb/Pt-Au-3DGR/CILE) was proposed by using HPPF$_6$ based CILE as the substrate electrode and Pt-Au-3DGR nanocomposite as the modifiers. The synthesized Pt-Au-3DGR was loaded with uniform size Pt and Au particles on its internal and external surfaces. Owing to the special pore structure of Pt-Au-3DGR, the whole conductivity, the specific surface area and Mb loading capacity are increased. The interaction of Pt-Au-3DGR and Mb improves the electron transfer rate between Fe(III)/Fe(II) in Mb molecule and CILE surface, which makes the direct electrochemical behavior in Mb molecule easier to be enhanced. Fourier transform infrared spectrum and ultraviolet spectrum show that the enzyme-like structure of Mb in Pt-Au-3DGR composite membrane is not damaged and its biological activity is maintained. At last, electrocatalysis of this electrochemical sensor to TCA and NaNO$_2$ was studied in detail, which proved that Nafion/Mb/Pt-Au-3DGR/CILE could be used in the development of third generation electrochemical biosensor.

References

1. J. C. Kendrew, *Science,* 139 (1963) 1259.
2. B. A. Wittenberg, J. B. Wittenberg, Annu. *Rev. Physiol.,* 51 (1989) 857.
3. M. W. Merx, U. Flogel, T. Stumpe, A. Godecke, U. K. Decking, J. Schrader*, FASEB J.,* 15 (2001) 1077.
4. T. Rassaf, U. Flogel, C. Drexhage, U. Hendgencotta, M. Kelm, J. Schrader, *Circ. Res.,* 100 (2007) 1749.
5. U. Flogel, M. W. Merx, A. Godecke, U.K. Decking, J. Schrader, *Proc. Natl. Acad. Sci. USA,* 98 (2001) 735.
6. A. H. Liu, M. D. Wei, I. Honma, H. S. Zhou, *Anal. Chem.,* 77 (2005) 8068.
7. H. Xie, X. Y. Li, G. L Luo, Y. Y. Niu, R. Y. Zou, C. X. Yin, S. M. Huang, W. Sun, G. J. Li, *Diamond Relat. Mater.,* 97 (2019) 107453.
8. Y. Y Niu, H. Xie, G. L Luo, W. J Weng, C. X. Ruan, G. J. Li, W. Sun, *RSC Adv.,* 9 (2019) 4480.
9. G. L Luo, H. Xie1, Y. Y Niu, J. Liu, Y. Q Huang, B. H Li, G. J Li, W. Sun, *Int. J. Electrochem. Sci.,* 14 (2019) 2405.
10. W. Q. Shen, F. E. Huggins, N. Shah, G. Jacobs, Y. Wang, X. Shi, G. P. Huffman, *Appl. Catal. A: Gen.,* 351 (2008) 102.
11. N. S. Anuar, W. J. Basirun, M. Ladan, M. Shalauddin, M. S. Mehmood, *Sens. Actuators B,* 266 (2018) 375.

Int. J. Electrochem. Sci., 16 **(2021)** Article Number: 211039

10

12. H Xie, Y. Y Niu, Y Deng, H. Cheng, C. X Ruan, G. J Li, W Sun, *J. Chin. Chem. Soc.*, 68 (2020) 1.
13. B. Su, W. Guo, L. Jiang, *Small,* 11 (2015) 1072.
14. N. Sofiaanuar, J. B. Wan, M. Shalauddin, S. Akhter, *RSC Adv.,* 10 (2020) 17336.
15. F. Zhang, Y. H. Li, J. Y. Li, Z. R. Tang, Y. J. Xu, *Environm. Pollution,* 253 (2019) 365.
16. L. Jiang, Z. Fan, *Nanoscale,* 6 (2014) 1922.
17. K. Chen, L. Chen, Y. Chen, H. Bai, L. Li, *J Mater. Chem.*, 22 (2012) 20968.
18. L. Li, S. He, M. Liu, C. Zhang, W. Chen, *Anal. Chem.*, 87 (2015) 1638.
19. Y. Ma, Y. Chen, *Natl. Sci. Rev.,* 2 (2015) 40.
20. Z. Chen, W. Ren, L. Gao, B. Liu, S. Pei, H. M. Cheng, *Nat. Mater.,* 10 (2011) 424.
21. O. T. Picot, V. G. Rocha, C. Ferraro, N. Ni, E. D. Elia, S. Meille, J. Chevalier, T. Saunders, T. Peijs, M. J. Reece, E. Saiz, *Nat. Commun.,* 8 (2017) 14425.
22. M. Hao, W. Zeng, Y. Q. Li, Z. C. Wang, *Rare Met.,* 40 (2021) 1494.
23. W. Chen, W. Weng, X. Niu, X. Li, Y. Men, W. Sun, G. Li, L. Dong, *J. Electroanal. Chem.,* 823 (2018) 137.
24. P. George, G. I. H. Hanania, *J. Biochem.,* 55 (1953) 236.
25. D. M. Byler, H. Susi, *Biopolymers,* 25 (1986) 469.
26. R. Y. Zou, X. B. Li, G. L Luo, Y. Y. Niu, W. J. Weng, W. Sun, J. W. Xi, Y. Chen, G. J. Li, *Electroanalysis,* 31 (2019) 575.
27. R. A. Kamin, G. S. Wilson, *Anal. Chem.,* 52 (1980) 1198.
28. G. Y. Chen, H. Sun, S. F. Hou, *Anal. Biochem.*,502 (2016) 43.
29. Y. Y. Niu, X. Y Li, H. Xie, G. L. Luo, R. Y. Zou, Y. R. Xi, G. J. Li, W. Sun, *J. Chin. Chem. Soc.*, 67 (2020) 1054.
30. H. Yan, X. Chen, Z. Shi, Y. Feng, J. Li, Q. Lin, X. Wang, W. Sun, *J. Solid State Electr.*, 20 (2016) 1783.
31. Z. Wen, W. Zhao, X. Li, X. Niu, X. Wang, L. Yan, X. Zhang, G. Li, W. Sun, *Int. J. Electrochem. Sci.*, 12 (2017) 2306.
32. Y. Deng, Z. R. Wen, G. L. Luo, H. Xie, J. Liu, Y. R. Xi, G. J. Li, W. Sun, *Curr. Anal. Chem.*, 16 (2020) 703.
33. J. Liu, W. J. Weng, H. Xie, G. L. Luo, G. J. Li, W. Sun, C. X. Ruan, X. H. Wang, *ACS Omega*, 4 (2019) 15653.
34. F. Shi, L. J. Yan, X. Q. Li, C. L. Feng, C. Z. Wang, B. X. Zhang, W. Sun, *J. Chin. Chem. Soc.*, (2021). (Online. DOI: 10.1002/jccs.202100123)
35. H. Xie, G. L. Luo, Y. Y. Niu, W. J. Weng, Y. X. Zhao, Z. Q Ling, C. X. Ruan, G. J. Li, W Sun, *Mater. Sci. Engi. C*, 107 (2020) 110209.